Coordinating the Motion of Labeled Discs with Optimality Guarantees under Extreme Density

Rupesh Chinta[1] and Shuai D. Han[2] and Jingjin Yu[2]

[1] Department of Electrical and Computer Engineering, Rutgers University
[2] Department of Computer Science, Rutgers University
{rupesh.chinta, shuai.han, jingjin.yu}@rutgers.edu

Abstract. We push the limit in planning collision-free motions for routing uniform labeled discs in two dimensions. First, from a theoretical perspective, we show that the constant-factor time-optimal routing of labeled discs can be achieved using a polynomial-time algorithm with robot density over 50% in the limit (i.e., over half of the workspace may be occupied by the discs). Second, from a more practical standpoint, we provide a high performance algorithm that computes near-optimal (e.g., $1.x$) solutions under the same density setting.

1 Introduction

The routing of rigid bodies (e.g., mobile robots) to desired destinations under dense settings (i.e., many rigid bodies in a confined workspace) is a challenging yet high utility task. On the side of computational complexity, when it comes to feasibility (i.e., finding collision-free paths for moving the bodies without considering path optimality), it is well known that coordinating the motion of translating rectangles is PSPACE-hard [8] whereas planning for moving labeled discs of variable sizes is strongly NP-hard in simple polygons [15]. More recently, it is further established that PSPACE-hardness extends to the unlabeled case as well [13]. Since computing an arbitrary solution is already difficult under these circumstances, finding optimal paths (e.g., minimizing the task completion time or the distances traveled by the bodies) are at least equally hard. Taking a closer look at proof constructions in [8, 13, 15], one readily observes that the computational difficulty increases as the bodies are packed more tightly in the workspace. On the other hand, in many multi-robot applications, it is desirable to have the capacity to have many robots efficiently and (near-)optimally navigate closely among each other, e.g., in automated warehouses [3, 19]. Provided that per-robot efficiency and safety are not compromised, having higher robot density directly results in space and energy[3] savings, thus enhancing productivity.

As a difficult but intriguing geometric problem, the optimal routing of rigid bodies has received much attention in many research fields, particularly robotics. While earlier research in the area tends to focus on the structural properties and complete (though not necessarily scalable) algorithmic strategies [4, 5, 10–12],

[3] With higher robot density, a fixed number of robots can fit in a smaller workspace, reducing the distance traveled by the robots

more recent studies have generally attempted to provide efficient and scalable algorithms with either provable optimality guarantees or impressive empirical results, or both. For the unlabeled case, a polynomial-time algorithm from [17] computes trajectories for uniform discs which minimizes the maximal path length traveled by any disc. The completeness of the algorithm depends on some clearance assumptions between the discs and between a disc and the environment. In [14], a polynomial-time complete algorithm is also proposed for unlabeled discs that optimizes the total travel distance, with a more natural clearance assumption compared to [17]. The clearance assumption (among others, the distance between two unit discs is at least 4) translates to a maximum density of about 23%, i.e., the discs may occupy at most 23% of the available free space. For the labeled case, under similar clearance settings, an integer linear programming (ILP) based method is provided in [22] for minimizing solution makespan. Though without polynomial running time guarantee, the algorithm is complete and appears to performs well in practice. Complete polynomial-time algorithms also exist that do not require any clearance in the start and goal configurations [7]. However, the supported density is actually lower in this case, as the algorithm needs to expand the start and goal configurations so that the clearance conditions in [22] is satisfied.

In this work, we study the problem of optimally routing labeled uniform unit discs in a bounded continuous two-dimensional workspace. As the main result, we provide a complete, deterministic, and polynomial-time algorithm that allows more than half of the workspace to be occupied by the discs while simultaneously ensuring $O(1)$ (i.e., constant-factor) time optimality of the computed paths. We also provide a practical and fast algorithm for the same setting without the polynomial running time guarantee. More concretely, our study brings the following contributions: *(i)* We show that, using a computer-based proof, when the distance between the centers of any two labeled unit discs is more than $\frac{8}{3}$, the continuous problem can be transformed into a multi-robot routing problem on a triangular grid graph with minimal optimality loss. A separation of $\frac{8}{3}$ implies a maximum density of over 50%. *(ii)* We develop a low polynomial-time constant-factor time-optimal algorithm for routing discs on a triangular grid with the constraint that no two discs may travel on the same triangle concurrently. The algorithm has a similar computation time as [7]: it can solve problem instances with thousands of robots. *(iii)* We develop a fast and novel integer linear programming (ILP) based algorithm that computes time-optimal routing plans for the triangular grid-based multi-robot routing problem. Combining *(i)* and *(ii)* yields the $O(1)$ time-optimal algorithm while combining *(i)* and *(iii)* results in the more practical and highly optimal algorithm. In addition, the $\frac{8}{3}$ separation proof employs both geometric arguments and computation-based verification, which may be of independent interest.

Our work leans on graph-theoretic methods for multi-robot routing, e.g., [1, 2, 9, 16, 18, 20, 21]. In particular, our constant-factor time-optimal routing algorithm for the triangular grids adapts from a powerful routing method for rectangular grid in [20] that actually works for arbitrary dimensions. However,

while the method from [20] comes with strong theoretical guarantee and runs in low polynomial time, the produced paths are not ideal due to the large constant factor. This prompts us to also look at more practical algorithms and we choose to build on the fast ILP-based method from [21], which allows us to properly encode the additional constraints induced by the triangular grid, i.e., no two discs may simultaneously travel along any triangle.

Organization. The rest of the paper is organized as follows. We provide a formal statement of the routing problem and its initial treatment in Section 2. In Section 3, we show how the problem may be transformed into a discrete one on a special triangular grid. Then, in Section 4 and Section 5, we present a polynomial time algorithm with $O(1)$-optimality guarantee and a fast algorithm that computes highly optimal solutions, respectively. We conclude in Section 6.

2 Preliminaries

2.1 Labeled Disc Routing: Problem Statement

Let $\mathcal{W}$ denote a closed and bounded $w \times h$ rectangular region. For technical convenience, we assume $w = 4n_1 + 2$ and $h = \frac{4}{\sqrt{3}}n_2 + 2$ for integers $n_1 \geq 2$ and $n_2 \geq 3$. There are n labeled unit discs residing in $\mathcal{W}$. Also for technical reasons, we assume that the discs are open, i.e., two discs are not in collision when their centers are exactly distance two apart. These discs may move in any direction with an instantaneous velocity v satisfying $|v| \in [0, 1]$. Let $\mathcal{C}_f \subset \mathbb{R}^2$ denote the free configuration space for a single robot in $\mathcal{W}$. The centers of the n discs are initially located at $\mathcal{S} = \{s_1, \ldots, s_n\} \subset \mathcal{C}_f$, with goals $\mathcal{G} = \{g_1, \ldots, g_n\} \subset \mathcal{C}_f$. For all $1 \leq i \leq n$, a disc labeled i initially located at s_i must move to g_i.

Beside planning collision-free paths, we want to optimize the resulting path quality by minimizing the *global task completion time*, also commonly known as the *makespan*. Let $P = \{p_1, \ldots, p_n\}$ denote a set of feasible paths with each p_i a continuous function, defined as

$$p_i : [0, t_f] \to C_f, p_i(0) = s_i, p_i(t_f) = g_i, \tag{1}$$

the makespan objective seeks a solution that minimizes t_f. That is, denoting $\mathcal{P}$ as the set of all feasible solution path sets, the task is to find a set P with $t_f(P)$ approaching the optimal solution

$$t_{min} := \min_{P \in \mathcal{P}} t_f(P). \tag{2}$$

Positive separation between the labeled discs is necessary to render the problem feasible (regardless of optimality). In this work, we require the following clearance condition between a pair of s_i and s_j and a pair of g_i and g_j:

$$\forall 1 \leq i, j \leq n, \quad \|s_i - s_j\| > \frac{8}{3}, \ \|g_i - g_j\| > \frac{8}{3}. \tag{3}$$

For notational convenience, we denote the problem address in this work as the *Optimal Labeled Disc Routing* problem (OLDR). By assumption (3) and

assuming that the unit discs occupy the vertices of a regular triangular grid, the discs may occupy $(\frac{1}{2}\pi * 1^2)/(\frac{1}{2}\frac{8}{3} * \frac{4}{\sqrt{3}}) \approx 51\%$ of the free space in the limit (to see that this is the case, we note that each equilateral triangle with side length $\frac{8}{3}$ contains half of a unit disc; each corner of the triangle contains $\frac{1}{6}$ of a disc).

2.2 Workspace Discretization

Similar to [4, 11, 12, 22], we approach OLDR through first discretizing the problem, starting by embedding a discrete graph within $\mathcal{W}$. The assumption of $w = 4n_1 + 2$ and $h = \frac{4}{\sqrt{3}}n_2 + 2$ on the workspace dimensions allows the embedding of a triangular grid with side length of $\frac{4}{\sqrt{3}}$ in $\mathcal{W}$ such that the grid has $2n_1$ columns and about n_2 (zigzagging) rows of equilateral triangles, and a clearance of 1 from $\partial\mathcal{W}$. An example is provided in Fig. 1.

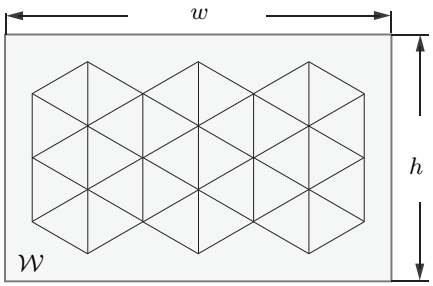

Fig. 1: An example of a workspace $\mathcal{W}$ with $w = 14$ and $h = 3\frac{4}{\sqrt{3}} + 2$, i.e., $n_1 = 3$ and $n_2 = 3$. The embedded triangular grid is at least distance 1 from the boundary of $\mathcal{W}$. The grid has 6 columns and 2+ zigzagging rows.

Throughout the paper, we denote the underlying graph of the triangular grid as G. Henceforth, we assume such a triangular grid G for a given workspace $\mathcal{W}$. The choice of the side length of $\frac{4}{\sqrt{3}}$ for the triangular grid ensures that two unit discs located on adjacent vertices of G may move simultaneously on G without collision when the angle formed by the two traveled edges is not sharp (Fig. 2).

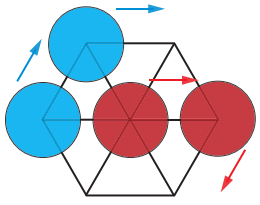

Fig. 2: On a triangular grid with a side length of $\frac{4}{\sqrt{3}}$, two unit discs, initially residing on two adjacent vertices of the grid, may travel concurrently on the grid without collision when the two trajectories do not form a sharp angle. In the figure, the two cyan discs may travel as indicated without incurring collision. On the other hand, the red discs will collide if they follow the indicated travel directions.

We note that $w \geq 10$ and $h \geq 3\frac{4}{\sqrt{3}} + 2$ are needed for our algorithm to have completeness and optimality guarantees. For smaller w or h, an instance may not be solvable. On the other hand, the discrete increment assumption on w and h are for technical convenience and are not strictly necessary. Without these discrete increments assumptions, we will need additional (and more complex) clearance assumptions between the discs and $\partial\mathcal{W}$, which does not affect the 51% density bound since $\partial\mathcal{W}$ contributes $\Theta(w+h)$ to the area of $\mathcal{W}$ which is wh. The ratio is $\Theta(\frac{w+h}{wh})$ which goes to zero as both w and h increase. We also mention that although this study only considers bounded rectangular workspace without static obstacles within the workspace, our results can be directly combined with [22] to support static obstacles.

3 Translating Continuous Problems to Discrete Problems with Minimal Penalty on Optimality

A key insight enabling this work is that, under the separation condition (3), a continuous OLDR can be translated into a discrete one with little optimality penalty. The algorithm for achieving this is relatively simple. For a given $\mathcal{W}$ and the corresponding $G = (V, E)$ embedded in $\mathcal{W}$, for each $s_i \in \mathcal{S}$, let $v_i^s \in V$ be a vertex of G that is closest to s_i (if there are more than one such v_i^s, pick an arbitrary candidate). After all v_i^s's (let $V_\mathcal{S} = \{v_i^s\}$) are identified for $1 \leq i \leq n$, let $d_{\max} = \max_i \parallel v_i^s - s_i \parallel$. Note that $d_{\max} \leq \frac{4}{3}$. We then let the labeled discs at s_i move in a straight line to the corresponding v_i^s at a constant speed given by $\frac{\|v_i^s - s_i\|}{d_{\max}}$, which means that for all $1 \leq i \leq n$, disc i will reach v_i^s in exactly one unit of time. The same procedure is then applied to $\mathcal{G}$ to obtain $V_\mathcal{G} = \{v_i^g\}$. The discrete OLDR is fully defined by $(G, V_\mathcal{S}, V_\mathcal{G})$. We denote the algorithm as DiscretizeOLDR. Fig. 3 illustrates the assignment of a few unit discs to vertices of the triangular grid.

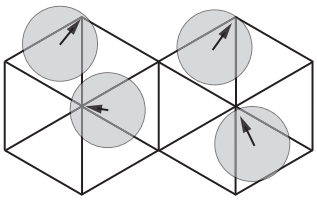

Fig. 3: An illustration of assigning a few unit discs to vertices of the triangular grid.

Because it takes a constant amount computational effort to deal with one disc, DiscretizeOLDR runs in linear time, i.e.,

Proposition 1. DiscretizeOLDR *has a running time of* $O(n)$.

The rest of this section is devoted to showing that DiscretizeOLDR is collision-free and incurs little penalty on time optimality. We only need to show this for translating $\mathcal{S}$ to $V_\mathcal{S}$; translating $\mathcal{G}$ to $V_\mathcal{G}$ is a symmetric operation. We first make the straightforward observation that DiscretizeOLDR adds a makespan penalty of up to four because translating $\mathcal{S}$ to $V_\mathcal{S}$ takes exactly one unit of time. Same holds for translating $\mathcal{G}$ to $V_\mathcal{G}$.

Proposition 2. DiscretizeOLDR *incurs a makespan penalty of up to four.*

We then show DiscretizeOLDR assigns a unique $v_i^s \in V$ for a given $s_i \in S$.

Lemma 1. DiscretizeOLDR *assign a unique* $v_i^s \in V$ *for an* $s_i \in S$.

Proof. Each equilateral triangle in G has a side length of $\frac{4}{\sqrt{3}}$, which means that the distance from the center of a triangle to its vertices is $\frac{4}{3}$. Therefore, for any $s_i \in S$, it must be at most of distance $\frac{4}{3}$ to at least one vertex of G. Let this vertex be v_i^s. Now given any other $s_j \in \mathcal{S}$, assume DiscretizeOLDR assigns to it v_j^s. We argue that $v_i^s \neq v_j^s$ because otherwise

$$\frac{4}{3} + \frac{4}{3} \geq \| v_i - v_i^s \| + \| v_j - v_j^s \| = \| v_i - v_i^s \| + \| v_j - v_i^s \| \geq \| v_i - v_j \| > \frac{8}{3},$$

which is a contradiction. Here, the first $\geq$ holds because $\| v_i - v_i^s \| \leq \frac{4}{3}$ and $\| v_j - v_j^s \| \leq \frac{4}{3}$ by DiscretizeOLDR; the second $\geq$ is due to the triangle inequality. The $>$ is due to assumption (3). □

Next, we establish that DiscretizeOLDR is collision-free. For the proof, we use geometric arguments assisted with computation-based case analysis.

Theorem 1. DiscretizeOLDR *guarantees collision-free motion of the discs.*

Proof. We fix a vertex $v \in V$ of the triangular grid G. By Lemma 1, at most one $s_i \in \mathcal{S}$ may be matched with v, in which case v becomes v_i^s. If this is the case, then s_i must be located within one of the six equilateral triangles surrounding v. Assume without loss of generality that s_i belongs to an equilateral triangle $\triangle uvw$ as shown in Fig. 4(a). The rules of DiscretizeOLDR further imply that s_i must fall within one (e.g., the orange shaded triangle in Fig 4 (a)) of the six triangles belonging to $\triangle uvw$ that are formed by the three bisectors of $\triangle uvw$. Let this triangle be $\triangle vox$. Now, let $s_j \neq s_i$ be the center of a labeled disc j; assume that disc j go to some $v_j^s \in V$. By symmetry, if we can show that disc i with $s_i \in \triangle vox$ and an arbitrary disc j with $\| s_i - s_j \| > \frac{8}{3}$ will not collide with each other as disc i and disc j move along $s_i v_i^s$ and $s_j v_j^s$, respectively, then DiscretizeOLDR is a collision-free procedure.

We then observe that if disc i and disc j collide as we align their centers to vertices of the triangular grid, then the distance between their centers must be exactly $\frac{8}{3}$ at some point before they collide (when their centers are of distance less than 2). Following this reasoning, instead of showing a disc j with $\| s_i - s_j \| > \frac{8}{3}$ will not collide with disc i, it suffices to show the same only for $\| s_i - s_j \| = \frac{8}{3}$. That is, for any $s_i \in \triangle vox$ and any s_j on a circle of radius $\frac{8}{3}$ centered at s_i, disc i and disc j will not collide as s_i and s_j move to v_i^s and v_j^s, respectively, according to the rules specified by DiscretizeOLDR (see Fig. 4(b) for an illustration).

To proceed from here, one may attempt direct case-by-case geometric analysis, which appears to be quite tedious. We instead opt for a more direct computer assisted proof as follows. We first partition $\triangle vox$ using axis-aligned square grids with side length ε; ε is some parameter to be determined through computation. For each of the resulting $\varepsilon \times \varepsilon$ square region (a small green square in Fig. 5),

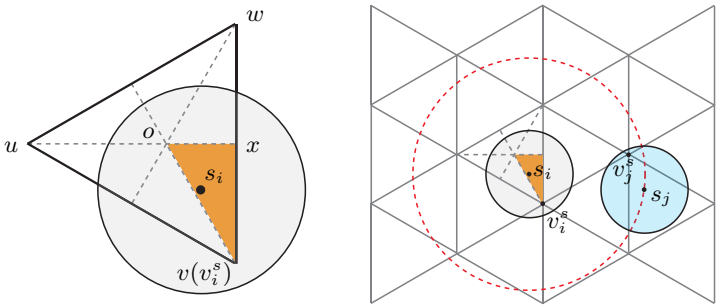

(a) (b)

Fig. 4: (a) By symmetry, for an $s_i \in \mathcal{S}$ to be moved to some $v = v_i^s$, we only need to consider the region $\triangle vox$, which is $\frac{1}{12}$-th of all possible places where s_i may appear. (b) For a fixed s_i, we only need to consider s_j that is of exactly $\frac{8}{3}$ distance from it.

we assume that s_i is at its center. For each fixed s_i, an annulus centered at s_i with inner radius $\frac{8}{3} - \frac{\sqrt{2}\varepsilon}{2}$ and outer radius $\frac{8}{3} + \frac{\sqrt{2}\varepsilon}{2}$ is obtained (part of which is illustrated as in Fig. 5). Given this construction, for any potential s_i' in a fixed $\varepsilon \times \varepsilon$ square, a circle of radius $\frac{8}{3}$ around it falls within the annulus.

We then divide the outer perimeter of the annulus into arcs of length no more than $\sqrt{2}\varepsilon$. For each piece, we obtain a roughly square region with side length $\sqrt{2}\varepsilon$ on the annulus, one of which is shown as the red square in Fig. 5. We take the center of the square as s_j. We then fix v_j^s accordingly (note that it may be the case that v_j^s is not unique for the square that bounds a piece of arc, in which case we will attempt all potentially valid v_j^s's).

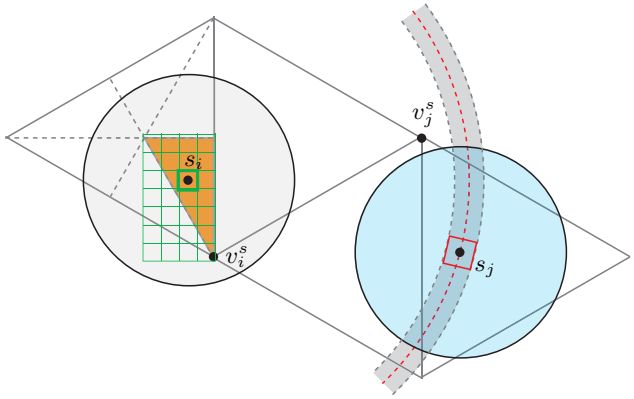

Fig. 5: Illustration of picking a pair of s_i and s_j for a computer based proof.

For each fixed set of s_i, v_i^s, s_j, and v_j^s, following the rules of DiscretizeOLDR, we may (analytically) compute the shortest distance between the centers of disc i and disc j as disc i is moved from s_i to v_i^s while disc j is moved from s_j to v_j^s. Let the trajectory followed by the two centers in this case be $\tau_i(t)$ and $\tau_j(t)$, respectively, with $0 \le t \le 1$ (as guaranteed by DiscretizeOLDR). We may express the distance (for fixed ε, s_i, v_i^s, s_j, and v_j^s) as $\delta_\varepsilon(s_i, s_j) = \min_t \| \tau_i(t) - \tau_j(t) \|$. For any s_i' that falls in the same $\varepsilon \times \varepsilon$ box as s_i, if disc i is

initially located at s'_i, let it follow a trajectory $\tau'_i(t)$ to v^s_i. We observe that $\| \tau_i(t) - \tau'_i(t) \| \leq \varepsilon$. This holds because as the center of disc i moves from anywhere within the $\varepsilon \times \varepsilon$ box to v^s_i, $\| \tau_i(t) - \tau'_i(t) \|$ continuously decreases until it becomes zero at v^s_i, which is the same for both s_i and s'_i. Therefore, the initial uncertainty is the largest, which is no more than ε because $\| s_i - s'_i \| \leq \frac{\sqrt{2}\varepsilon}{2}$. The same argument applies to disc j, i.e., $\| \tau_j(t) - \tau'_j(t) \| \leq \varepsilon$. Therefore, we have

$$\begin{aligned}
\delta_\varepsilon(s_i, s_j) &= \min_t \| \tau_i(t) - \tau_j(t) \| \\
&= \min_t \| \tau_i(t) - \tau'_i(t) + \tau'_j(t) - \tau_j(t) + \tau'_i(t) - \tau'_j(t) \| \\
&\leq \min_t (\| \tau_i(t) - \tau'_i(t) \| + \| \tau'_j(t) - \tau_j(t) \| + \| \tau'_i(t) - \tau'_j(t) \|) \\
&\leq 2\varepsilon + \min_t \| \tau'_i(t) - \tau'_j(t) \| \\
&\leq 2\varepsilon + \delta_\varepsilon(s'_i, s'_j).
\end{aligned}$$

If $\delta_\varepsilon(s_i, s_j) > 2\varepsilon$, then we may conclude that $\delta_\varepsilon(s'_i, s'_j) > 0$. We verify this using a python program that computes the minimum $\delta_\varepsilon(s_i, s_j)$ over all possible choices of s_i and s_j given a small ε. When $\varepsilon = 0.025$, we obtain that $\delta_\varepsilon(s_i, s_j)$ is lower bounded at approximately 0.076, which is larger than $2\varepsilon = 0.05$. Therefore, DiscretizeOLDR is a collision-free algorithm. □

With DiscretizeOLDR, in Section 4 and Section 5, we assume a discrete multi-robot routing problem is given as a 3-tuple $(G, V_\mathcal{S}, V_\mathcal{G})$ in which G is the unique triangular grid embedded in $\mathcal{W}$. Also, $V_\mathcal{S}, V_\mathcal{G} \subset V$ and $|V_\mathcal{S}| = |V_\mathcal{G}| = n$.

4 Constant-Factor Time-Optimal Multi-Robot Routing on Triangular Grid

In [20], it is established that constant-factor makespan time-optimal solution can be computed in quadratic running time on a k-dimensional orthogonal grid G for an arbitrary fixed k. It is a surprising result that applies even when $n = |V|$, i.e., there is a robot or disc on every vertex of grid G. The functioning of the algorithm, PaF (standing for *partition and flow*), requires putting together many algorithmic techniques. However, the key requirements of the PaF algorithm hinges on three basic operations, which we summarize here for the case of $k = 2$. Due to limited space, only limited details are provided.

First, to support the case of $n = |V|$ while ensuring desired optimality, it must be possible to "swap" two adjacent discs in a constant sized neighborhood in a constant number of steps (i.e. makespan), as illustrated in Fig. 6. This operation is essential in ensuring makespan time optimality as the locality of the operation allows many such operations to be concurrently carried out. Note that a random problem on G is always feasible if G satisfies this requirement, because any two robots can exchange their locations without affecting the other robots by using multiple "swap" actions.

Second, it must be possible to iteratively *split* the initial problem into smaller sub-problems. This is achieved using a *grouping* operation that in turn depends

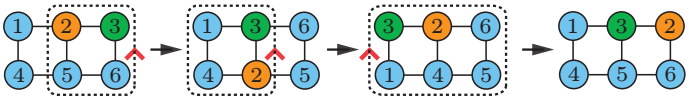

Fig. 6: Discs 2 and 3 may be "swapped" in three steps on a 3×2 grid, implying that any two discs can be swapped in $O(1)$ steps without net effect on other discs.

on the swap operation. We illustrate the idea using an example. In Fig. 7(a), a 8×4 grid is split in the middle into two smaller grids. Each vertex is occupied by a disc; we omit the individual labels. The lightly (cyan) shaded discs have goals on the right 4×4 grid. The grouping operation moves the 7 lightly shaded discs to the right, which also forces the 7 darker shaded discs on the right to the left side. This is achieved through multiple rounds of concurrent swap operations either along horizontal lines or vertical lines. The result is Fig. 7(b). This effectively reduces the initial problem $(G, V_{\mathcal{S}}, V_{\mathcal{G}})$ to two disjoint sub-problems. Repeating the iterative process can actually solve the problem completely but does not always guarantee constant-factor makespan time optimality in the worst case. This is referred to as the iSAG algorithm in [20].

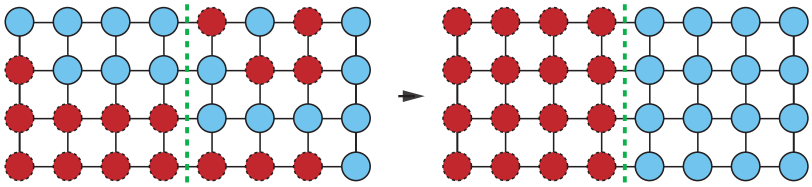

Fig. 7: Illustration of an iteration of the iSAG algorithm.

Lastly, PAF achieves guaranteed constant-factor optimality using iSAG as a subroutine. It begins by computing the maximum distance between any pair of $v_i^s \in V_{\mathcal{S}}$ and $v_i^g \in V_{\mathcal{G}}$ over all $1 \leq i \leq n$. Let this distance be d_g. G is then partitioned into square grid *cells* of size roughly $5d_g \times 5d_g$ each. With this partition, a disc must have its goal in the same cell it is in or in a neighboring cell. After some pre-processing using iSAG, the discs that need to cross cell boundaries can be arranged to be near the destination cell boundary. At this point, multiple global circulations (a circulation may be interpreted as discs rotating synchronously on a cycle on G) are arranged so that every disc ends up in a $5d_g \times 5d_g$ cell partition where its goal also resides. A rough illustration of the global circulation concept is provided in Fig. 8. Then, a last round of iSAG is invoked at the cell level to solve the problem, which yields a constant-factor time-optimal solution even in the worst case.

To adapt PAF to the special triangular grid graph G, we need to: *(i)* identify a constant sized local neighborhood for the swapping operation to work, *(ii)* identify two "orthogonal" directions that cover G for the iSAG algorithm to work, and *(iii)* ensure that the constructed global circulation can be executed. Because of the limitation imposed by the triangular grid, i.e., any two edges of a triangle cannot be used at the same time (see Fig. 2), achieving these conditions simultaneously becomes non-trivial. In what follows, we will show how we may *simulate* PAF on a triangular grid G under the assumption that all vertices of

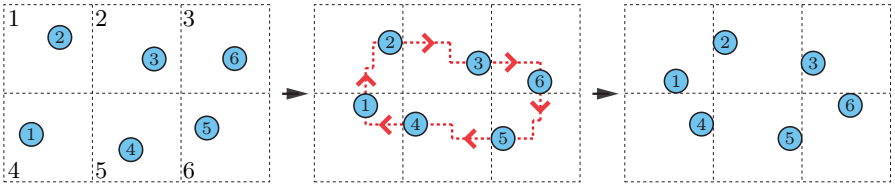

Fig. 8: Illustration of a single global circulation constructed and executed by PAF (the discs and the underlying grid cells are not fully drawn). (a) In six partitioned $(5d_g \times 5d_g)$ cells numbered $1-6$ in G, there are six labeled discs with goals in the correspondingly numbered cells, e.g., disc 1 should be in cell 1. (b) Using iSAG in each cell, discs $1-6$ are moved to boundary areas and a cycle is formed on G for robot routing. (c) Moving all discs on the cycle by one edge synchronously, all discs are now in the desired cell; no other discs (not shown) have crossed any cell boundary.

G are occupied by labeled discs, i.e., $n = |V|$. For the case of $n < |V|$, we may treat empty vertices as having "virtual discs" placed on them.

Because two edges of a triangle cannot be simultaneously used, we use two adjacent hexagons on G (e.g., the two red full hexagons in Fig. 9(a)) to simulate the two square cells in Fig. 6. It is straightforward to verify that the swap operation can be carried out using two adjacent hexagons. There is an issue, however, as not all vertices of G can be covered with a single hexagonal grid. For example, the two red hexagons in Fig. 9(a) left many vertices uncovered. This can be resolved using up to three sets of interweaving hexagon grids as illustrated in Fig. 9(a) (here we use the assumption that $\mathcal{W}$ has dimensions $w \geq 10$ and $h \geq 3\frac{4}{\sqrt{3}} + 2$, which limits the possible embeddings of the triangular grid G). We note that for the particular graph G in Fig. 9(a), we only need the red and the green hexagons to cover all vertices.

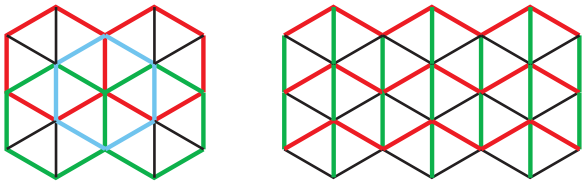

Fig. 9: (a) We may use the red, green, and cyan hexagon grids on G to perform the swap operation. (b) The red and green paths may serve as orthogonal paths for carrying out the split and group operations as required by iSAG.

To realize requirement *(ii)*, i.e., locating two sets of "orthogonal" paths for carrying out iSAG iterations, we may use the red and green paths as illustrated in Fig. 9(b). The remaining issue is that the red waving paths do not cover the few vertices at the bottom of G (the green paths, on the other hand, covers all vertices of G). This issue can be addressed with some additional swaps (e.g., with a second pass) which still only takes constant makespan during each iteration of iSAG and does not impact the time optimality or running time of iSAG.

The realization of requirement *(iii)* is straightforward as the only restriction here is that the closed paths for carrying out circulations on G cannot contain

sharp turns. We can readily realize this using any one of the three interweaving hexagonal grids on G that we use for the swap operation, e.g., the red one in Fig. 9(a). Clearly, any cycle on a hexagonal grid can only have angles of $\frac{2\pi}{3}$ which are obtuse. We note that there is no need to cover all vertices for this global circulation-based routing operation because only a fraction ($< \frac{1}{2}$, see [20] for details) of discs need to cross the $5d_g \times 5d_g$ cell boundary. On the other hand, any one of the three hexagonal grids cover about $\frac{2}{3}$ of the vertices on a large G.

Calling the adapted PAF algorithm on the special triangular grid as PAFT, we summarize the discussion in this section in the following result.

Lemma 2. PAFT *computes constant-factor makespan time-optimal solutions for multi-robot routing on triangular grids in* $O(|V|^2)$ *time.*

Combining DISCRETIZEOLDR with PAFT then gives us the following. In deriving the running time result, we use the fact that $wh = \Theta(|V|) = \Omega(n)$.

Theorem 2. *In a rectangular workspace* $\mathcal{W}$ *with* $w \geq 10$ *and* $h \geq 3\frac{4}{\sqrt{3}} + 2$*, for* n *labeled unit discs having start and goal configurations of separation no less than* $\frac{8}{3}$*, constant-factor makespan time-optimal collision-free paths connecting the two configurations may be computed in* $O(w^2h^2)$ *time.*

We conclude this section with the additional remark that PAFT should mainly be viewed as providing a theoretical guarantee rather than being a practical algorithm due to the fairly large constant in the optimality guarantee.

5 Fast Computation of Near-Optimal Solutions via Integer Linear Programming

From a practical standpoint, the DISCRETIZEOLDR algorithm introduces the possibility of plugging in any discrete algorithm for multi-robot routing. Indeed, algorithms including those from [1, 2, 16, 18, 21] may be modified to serve this purpose. In this paper, we develop a new integer linear programming (ILP) approach based on the time-expanded network structure proposed in [21]. The benefits of using an ILP model are its flexibility and computational performance when combined with the appropriate solvers, e.g., Gurobi [6].

5.1 Integer Linear Programming Model for Multi-Robot Routing on Triangular Grids

The essential idea behind an ILP-based approach, e.g., [21], is the construction of a directed time-expanded network graph representing the possible flow of the robots over time. Given a discrete problem instance $(G, V_{\mathcal{S}}, V_{\mathcal{G}})$, the network is constructed by taking the vertex set V of G and making $T+1$ copies of it. Each copy represents an integer time instance starting from 0 to T. Then, a directed edge is added between any two vertices when they are both adjacent on G and in time, in the direction from time step t to time step $t+1$.

To build the ILP model, we create a binary variable for each robot and each edge in the time-expanded graph to represent whether the given robot uses that edge as part of its trajectory. We then add constraints to ensure that robots will

not collide. The basic model from [21] only ensures that no two robots can use the same edge or vertex at the same time. But in our case, we need to consider more complex interactions, which are detailed as follows.

Denoting $N(i)$ as the set of vertex $i \in V$ and its neighbors, the ILP model contains two sets of binary variables: *(i)* $\{x_{r,i,j,t} | 1 \leq r \leq n, i \in V, j \in N(i), 0 \leq t < T\}$, where $x_{r,i,j,t}$ indicates whether robot r moves from vertex i to j between time step t and $t+1$. Note that by a reachability test, some variables here are fixed to 0. *(ii)* $\{x_{r,v_r^g,v_r^s,T} | 1 \leq r \leq n\}$ which represent virtual edges between the goal vertex of each robot at time step T and its start vertex at time 0. $x_{r,v_r^g,v_r^s,T}$ is set to 1 *iff* r reaches its goal at T. The objective of this ILP formulation is to maximize the number of robots that reach their goal vertices at T, i.e.,

$$\text{maximize} \sum_{1 \leq r \leq n} x_{r,v_r^g,v_r^s,T},$$

under the constraints

$$\forall 1 \leq r \leq n, 0 \leq t < T, \sum_{i \in N(j)} x_{r,i,j,t} = \sum_{k \in N(j)} x_{r,j,k,t+1}, \tag{4}$$

$$\forall 1 \leq r \leq n, \sum_{i \in N(v_r^s)} x_{r,v_r^s,i,0} = \sum_{i \in N(v_r^g)} x_{r,i,v_r^g,T-1} = x_{r,v_r^g,v_r^s,T}, \tag{5}$$

$$\forall 0 \leq t < T, i \in V, \sum_{1 \leq r \leq n} \sum_{j \in N(i)} x_{r,i,j,t} \leq 1, \tag{6}$$

$$\forall 0 \leq t < T, i \in V, j \in N(i), \sum_{1 \leq r \leq n} x_{r,i,j,t} + \sum_{1 \leq r \leq n} x_{r,j,i,t} \leq 1. \tag{7}$$

Here, constraint (4) and (5) ensure a robot always starts from its start vertex, and can only stay at the current vertex or move to an adjacent vertex at each time step. Moreover, constraint (5) is essential for calculating the objective value. Constraint (6) prevents robots from simultaneously occupying the same vertex, while constraint (7) eliminates head-to-head collisions on edges.

For a triangular grid, we must impose one extra set of constraints so that two robots cannot simultaneously move on the same triangle. Reasoning about each triangle formed by mutually adjacent vertices $i, j, k \in V$, for all $0 \leq t < T$, the constraint can be expressed as

$$\sum_{1 \leq r \leq n} (x_{r,i,j,t} + x_{r,j,i,t} + x_{r,i,k,t} + x_{r,k,i,t} + x_{r,j,k,t} + x_{r,k,j,t}) \leq 1. \tag{8}$$

Building on the ILP model, the overall route planning algorithm for triangular grids, TriILP, is outlined in Alg. 1. In line 1, an underestimated makespan T is computed by routing robots to goal vertices while ignoring mutual collisions. Then, as T gradually increases (line 6), ILP models are iteratively constructed and solved (line 3-4) until the resulting objective value *objval* equals n. In line 5, time-optimal paths are extracted and returned. Derived from [21], TriILP has completeness and optimality guarantees.

To improve the scalability of the ILP-based algorithm, a *k-way split heuristic* is introduced in [21] that adds intermediate robot configurations (somewhere between the start and goal configurations) to split the problem into sub-problems. These sub-problems require fewer steps to solve, which means that the corresponding ILP models are much smaller and can be solved much faster. Detailed description and evaluation of the split heuristic are avaliable in [21]. This heuristic is directly applicable to TriILP.

Algorithm 1: TriILP

```
1 T ←UnderestimatedMakespan(G, V_S, V_G)
2 while True do
3 |   model ← PrepareModel(G, V_S, V_G, T)
4 |   objval ← Optimize(model)
5 |   if objval equals to n then return ExtractSolution(model)
6 |   else T ← T + 1
```

5.2 Performance Evaluation

We evaluate the performance of TriILP based on two standard measures: *computation time* and *optimality ratio*. To compute the optimality ratio, we first obtain the *underestimated makespan* $\hat{t_i}$, which is the number of steps needed to move robots to their goals for a given problem instance i while ignoring potential robot-robot collisions. Denoting t_i as the makespan produced by TriILP of the i-th problem instance, the optimality ratio is defined as $(\sum_i t_i)/(\sum_i \hat{t_i})$. For each set of problem parameters, ten random instances are generated and the average is taken. All experiments are executed on an Intel® Core™ i7-6900K CPU with 32GB RAM at 2133MHz. For the ILP solver, Gurobi 8 is used [6].

We begin with TriILP on purely discrete multi-robot routing problems. On a densely occupied minimum triangular grid ($n_1 = 2, n_2 = 3, |V| = 22, n = 16$) as allowed by our formulation, a randomly generated problem can be solved optimally within 5 seconds on average. For a much larger environment ($n_1 = 7, n_2 = 16, |V| = 232$), we evaluate TriILP with k-way split heuristics, gradually increasing the number of robots. As shown in Fig. 10, TriILP could solve problems with 50 robots optimally in 60 seconds. Performance of TriILP is significantly improved with k-way split heuristic: with 4-way split, TriILP can solve problems with 110 robots in 55 seconds to 1.65-optimal. With 8-way split, we can further push to 140 robots with reasonable optimality ratio.

Solving (continuous) OLDR requires both DiscretizeOLDR and TriILP. We first attempted a scenario where the density approaches the theoretical limit by placing the robots just $\frac{8}{3}$ apart from each other in a regular (triangular) pattern for both start and goal configurations (see Fig. 11(a) for an illustration; we omit the labels of the robots, which are different for the start and goal

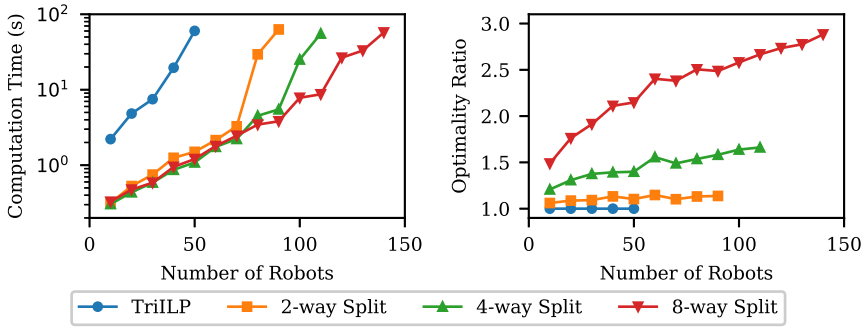

Fig. 10: Performance of TriILP with k-way split heuristics on a triangular grid with 232 vertices and varying numbers of robots.

configurations). After running DiscretizeOLDR, we get a discrete arrangement as illustrated in Fig. 11(b). For this particular problem, we can compute a 1.5-optimal solution in 2.1 second without using splitting heuristics.

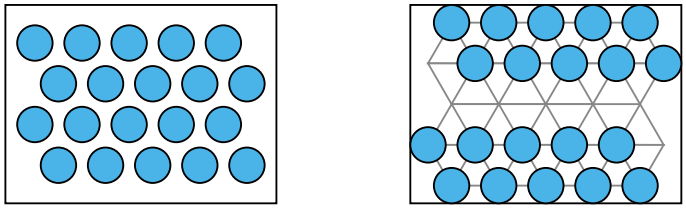

(a) (b)

Fig. 11: Illustration of a compact OLDR instance with 20 densely packed robots, and the configuration of robots after DiscretizeOLDR.

To test the effectiveness of combining DiscretizeOLDR and TriILP, we constructed many instances similar to Fig. 11 but with different environment sizes, always packing as many robots as possible with separation of exactly $\frac{8}{3}$. The computational performance of this case is compiled in Fig. 12. With the 8-way split heuristic, our method can solve tightly packed problems of 120 robots in 21.93 seconds with a 3.88 optimality ratio. We note that the (underestimated) optimality ratio in this case actually decreases as the number of robots increases. This is expected because when the number of robots are small, the corresponding environment is also small. The optimality loss due to discretization is more obvious when the environment is smaller.

A second evaluation of OLDR carries out a comparison between TriILP (plus DiscretizeOLDR) and HexILP (the main algorithm from [22], which is based on a hexagonal grid discretization). We fix $\mathcal{W}$ with $w = 42$ and $h = 43.57$; the number of vertices in the triangular grid and hexagonal grid are 312 and 252, respectively. For each fixed number of robots n, $\mathcal{S}$ and $\mathcal{G}$ are randomly generated within W that are at least $\frac{8}{3}$ apart. Note that this means that collisions may potentially happen for HexILP during the discretization phase, which are ignored (to our disadvantage). The evaluation result is provided in Fig. 13. Since discretization based on a triangular grid produces larger models, the running time

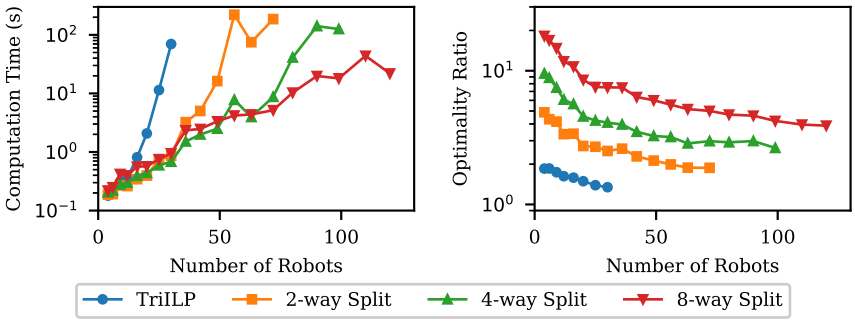

Fig. 12: Performance of TriILP (plus DiscretizeOLDR) on dense OLDR instances.

is generally a bit higher when compared with discretization based on hexagonal grids. However, TriILP can solve problems with many more robots and also produce solutions with much better optimality guarantees.

`https://youtu.be/2-QHESZ_p3E` illustrates a few typical runs of TriILP.

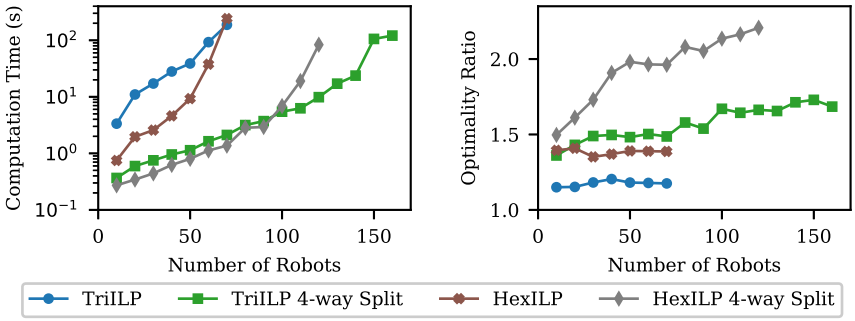

Fig. 13: Performance comparison between TriILP and HexILP (with and without 4-way split heuristic) on randomly generated OLDR instances with a fixed $\mathcal{W}$.

6 Conclusion and Future Work

In this work, we have developed a complete, polynomial-time algorithm for multi-robot routing in a bounded environment under extremely high robot density. The algorithm produces plans that are constant-factor time-optimal. We also provide a fast and more practical ILP-based algorithm capable of generating near-optimal solutions. We mention here that extensions to 3D settings, which may be more applicable to drones and other airborne robot vehicles, can be readily realized under the same framework with only minor adjustments.

Given the theoretical and practical importance of multi-robot (and more generally, multi-agent) routing in crowded settings, in future work, we would like to push robot density to be significantly higher than 50%. To achieve this while retaining optimality assurance, we believe the computation-based method developed in this work can be leveraged, perhaps in conjunction with a more sophisticated version of the DiscretizeOLDR algorithm. On the other hand, a triangular grid supports a maximum density of 66%; it may be of interest to explore alternatives structures for accommodating denser robot configurations.

Acknowledgement. This work is supported by NSF awards IIS-1617744 and IIS-1734419. Opinions or findings expressed here do not reflect the views of the sponsor.

References

1. Boyarski, E., Felner, A., Stern, R., Sharon, G., Betzalel, O., Tolpin, D., Shimony, E.: Icbs: The improved conflict-based search algorithm for multi-agent pathfinding. In: Eighth Annual Symposium on Combinatorial Search (2015)
2. Cohen, L., Uras, T., Kumar, T., Xu, H., Ayanian, N., Koenig, S.: Improved bounded-suboptimal multi-agent path finding solvers. In: International Joint Conference on Artificial Intelligence (2016)
3. Enright, J., Wurman, P.R.: Optimization and coordinated autonomy in mobile fulfillment systems. In: Automated action planning for autonomous mobile robots, pp. 33–38 (2011)
4. Erdmann, M.A., Lozano-Pérez, T.: On multiple moving objects. In: Proceedings IEEE International Conference on Robotics & Automation, pp. 1419–1424 (1986)
5. Ghrist, R., O'Kane, J.M., LaValle, S.M.: Computing Pareto Optimal Coordinations on Roadmaps. International Journal of Robotics Research **24**(11), 997–1010 (2005)
6. Gurobi Optimization, Inc.: Gurobi optimizer reference manual (2018)
7. Han, S.D., Rodriguez, E.J., Yu, J.: Sear: A polynomial-time expected constant-factor optimal algorithmic framework for multi-robot path planning. In: Proceedings IEEE/RSJ International Conference on Intelligent Robots & Systems (2018). To appear
8. Hopcroft, J.E., Schwartz, J.T., Sharir, M.: On the complexity of motion planning for multiple independent objects; PSPACE-hardness of the "warehouseman's problem". The International Journal of Robotics Research **3**(4), 76–88 (1984)
9. Kornhauser, D., Miller, G., Spirakis, P.: Coordinating pebble motion on graphs, the diameter of permutation groups, and applications. In: Proceedings IEEE Symposium on Foundations of Computer Science, pp. 241–250 (1984)
10. LaValle, S.M., Hutchinson, S.A.: Optimal motion planning for multiple robots having independent goals. IEEE Transactions on Robotics & Automation **14**(6), 912–925 (1998)
11. Peasgood, M., Clark, C., McPhee, J.: A complete and scalable strategy for coordinating multiple robots within roadmaps. IEEE Transactions on Robotics **24**(2), 283–292 (2008)
12. Solovey, K., Halperin, D.: k-color multi-robot motion planning. In: Proceedings Workshop on Algorithmic Foundations of Robotics (2012)
13. Solovey, K., Halperin, D.: On the hardness of unlabeled multi-robot motion planning. In: Robotics: Science and Systems (RSS) (2015)
14. Solovey, K., Yu, J., Zamir, O., Halperin, D.: Motion planning for unlabeled discs with optimality guarantees. In: Robotics: Science and Systems (2015)
15. Spirakis, P., Yap, C.K.: Strong NP-hardness of moving many discs. Information Processing Letters **19**(1), 55–59 (1984)
16. Standley, T., Korf, R.: Complete algorithms for cooperative pathfinding problems. In: Proceedings International Joint Conference on Artificial Intelligence (2011)
17. Turpin, M., Mohta, K., Michael, N., Kumar, V.: CAPT: Concurrent assignment and planning of trajectories for multiple robots. International Journal of Robotics Research **33**(1), 98–112 (2014)

18. Wagner, G., Choset, H.: M*: A complete multirobot path planning algorithm with performance bounds. In: Proceedings IEEE/RSJ International Conference on Intelligent Robots & Systems, pp. 3260–3267 (2011)
19. Wurman, P.R., D'Andrea, R., Mountz, M.: Coordinating hundreds of cooperative, autonomous vehicles in warehouses. AI Magazine **29**(1), 9–19 (2008)
20. Yu, J.: Constant factor time optimal multi-robot routing on high-dimensional grid. In: Robotics: Science and Systems (2018)
21. Yu, J., LaValle, S.M.: Optimal multi-robot path planning on graphs: Complete algorithms and effective heuristics. IEEE Transactions on Robotics **32**(5), 1163–1177 (2016)
22. Yu, J., Rus, D.: An effective algorithmic framework for near optimal multi-robot path planning. In: Robotics Research, pp. 495–511. Springer (2018)